miR-34a induces apoptosis and pyroptosis in D-Galactose-induced aging cochlear hair cells via inhibiting TFAM and promoting mitochondrial dysfunction *in vitro* and *in vivo*

YILAN WANG[1*], MING YANG[2*], GUIHUA WANG[1*], WEIMIN LIU[1], BIN DENG[1], XIAORAN YANG[1] and XUZHAO LI[3]

[1]Department of Otolaryngology Head and Neck Surgery, People's Hospital of Ningxia Hui Autonomous Region, Ningxia Medical University, Yinchuan, Ningxia Hui 750002, P.R. China; [2]Department of Emergency Medicine, People's Hospital of Ningxia Hui Autonomous Region, Ningxia Medical University, Yinchuan, Ningxia Hui 750002, P.R. China; [3]Department of General Surgery, People's Hospital of Ningxia Hui Autonomous Region, Ningxia Medical University, Yinchuan, Ningxia Hui 750002, P.R. China

Received July 2, 2024; Accepted January 2, 2025

DOI: 10.3892/ijmm.2025.5541

Abstract. Aging of the auditory system causes progressive hearing deficit and affects millions of people; however, the underlying mechanism remains largely unknown. D-galactose (D-gal)-induced aging models were established *in vitro* using HEI-OC1 cells and *in viv*o using C57BL/6 mice to investigate the role of miR-34a in age-related hearing loss (ARHL). HEI-OC1 cells were treated with D-gal for, while mice received daily intraperitoneal injections of D-gal for six weeks. Molecular and functional analyses, including reverse transcription-quantitative PCR, Western blot, flow cytometry, immunofluorescence, and dual-luciferase reporter assays, were performed to evaluate oxidative stress, mitochondrial dysfunction, apoptosis, and pyroptosis, with miR-34a inhibitor and DRP1 inhibitor (Mdivi-1) used to assess their regulatory effects. D-gal induced hair cell loss by apoptosis and pyroptosis, which was modulated by microRNA (miR)-34a via mitochondrial dysfunction *in vitro* and *in vivo*. Inhibition of mitochondrial transcription factor A (TFAM), which is the target gene of miR-34a, was involved in the underlying molecular mechanism. miR-34a mediated apoptosis and pyroptosis in D-gal-induced cochlear hair cells via inhibiting TFAM and promoting mitochondrial dysfunction *in vitro* and *in vivo* and may serve as a new potential target for future ARHL treatment.

Correspondence to: Professor Xiaoran Yang, Department of Otolaryngology Head and Neck Surgery, People's Hospital of Ningxia Hui Autonomous Region, Ningxia Medical University, 301 Zhengyuan North Street, Jinfeng, Yinchuan, Ningxia Hui 750002, P.R. China
E-mail: 18795381482@163.com

Professor Xuzhao Li, Department of General Surgery, People's Hospital of Ningxia Hui Autonomous Region, Ningxia Medical University, 301 Zhengyuan North Street, Jinfeng, Yinchuan, Ningxia Hui 750002, P.R. China
E-mail: 251170583@qq.com

*Contributed equally

Key words: age-related hearing loss, mitochondrial dysfunction, microRNA-34a, mitochondrial transcription factor A, pyroptosis

Introduction

The prevalence of age-related hearing loss (ARHL) is rising, with over two-thirds of adults aged ≥60 and older experiencing clinically significant hearing impairment worldwide (1). ARHL may cause progressive sensorineural hearing loss, impaired hearing sensitivity, and language discrimination (2), which may lead to late-life depression and cognitive decline (3). ARHL is linked to multiple risk factors, including genetic, noise and ototoxic drugs (4), making it a complex disorder that results from cumulative effects. Previous evidence has revealed that the predominant reason for ARHL is sensory inner and outer hair cell damage, which contradicts the long-accepted theory that impairment of the stria vascularis is the primary reason (5). Human autopsy specimens demonstrate that the degree of inner-ear sensory cell loss is positively associated with severity of hearing loss, indicating the importance of understanding the mechanism underlying cell loss since hair cells cannot regenerate (5).

Because of the slow and uncontrollable nature of the normal aging process, D-galactose (D-gal) is widely used to induce rapid aging in ARHL studies (6-8). D-gal is a reducing sugar that undergoes oxidation by galactose oxidase to aldehydes and hydrogen peroxide while present in excessive amounts, resulting in oxidative damage (9). Auditory dysfunction and corresponding pathological impairments in D-gal-treated rats and mice are similar to those observed in natural aging (10,11), making D-gal a viable approach to mimic aging *in vitro* and *in vivo*.

MicroRNAs (miRNAs or miRs) are non-coding RNAs, typically ~22 nucleotides in length, serving key regulatory roles in various biological processes. They can bind to mRNA targets to degrade mRNA or prevent mRNA translation into protein (12). Thus, miRNAs exert a negative regulatory effect

on the expression of genes or proteins and are involved in cellular processes, including development, differentiation, proliferation, autophagy and apoptosis. A miRNA triad (composed of miR-96, miR-182, and miR-183) was initially identified in zebrafish hair cells of sensory epithelia using *in situ* hybridization in 2005 (13). Numerous miRNAs, such as miR-96, -182 and -183, have been found to be highly expressed in the cochlea (14) and are considered as future therapeutic interventions for hearing loss, primarily ARHL (15). The present study aimed to identify key miRNAs that contribute to ARHL and the underlying mechanisms and regulatory pathways *in vitro* and *in vivo*.

Materials and methods

Animals and D-gal aging model. A total of 16 C57BL/6 mice (male; age, ~16 weeks; weight, 26-30 g) were obtained from Shanghai SLAC Laboratory Animal Co., Ltd. The mice were housed at 23˚C with 60% humidity with a 12/12-h light/dark cycle and free access to food and water. After adapting to the environment for seven days, mice were randomly divided into a control and an aging group (both n=8). D-gal (cat. no. G0625, Sigma-Aldrich; Merck KGaA) was dissolved in sodium carboxymethyl cellulose solution (CMC-Na; Sigma-Aldrich). Mice in the aging group received 150 mg/kg D-gal once daily (intraperitoneal injection) for six weeks. The control group was injected with CMC-Na without D-gal following the same schedule. Animal experiments were approved by the Ethics Committee for Animal Research (approval no. 2020-NZR-037, People's Hospital of Ningxia Hui Autonomous Region, Yinchuan, China) and performed in accordance with the Guide for the Care and Use of Laboratory Animals prepared by the National Academy of Sciences and published by the National Institutes of Health (16).

All mice were intraperitoneally injected with 30 mg/kg pentobarbital sodium and sacrificed by cervical dislocation. Death was verified by cessation of respiration and heartbeat. The cochleae were then collected. Fine forceps were used under a stereomicroscope to remove the stria vascularis and tectorial membranes. The apical organ of the Corti was used for further procedures. If any animal reached the predefined humane endpoints [loss of >20% of body weight; signs of pian and stress (piloerection, hunched posture, dehydration, sunken or closed eyes and self-isolation)], they were humanely euthanized. Animal health and behaviors were monitored daily. To avoid repeated damage to the same site, abdominal areas (left or right side) were alternated during daily injections, while avoiding proximity to internal organs.

Cell culture. House Ear Institute-Organ of Corti 1 (HEI-OC1) cells (cat. no. CVCL_D899, American Type Culture Collection) were cultured at 33˚C, 10% CO_2 in high-glucose DMEM containing 10% FBS (both Gibco; Thermo Fisher Scientific, Inc.) without antibiotics. D-gal was applied at a concentration of 5, 10 and 20 mg/ml for 72 h at 33˚C. For miR inhibitor transfection, HEI-OC1 cells were seeded in six-well plates at a density of $5x10^5$ cells/well and allowed to reach 60-70% confluency before transfection. Cells were transfected with 10 nM miR-34a inhibitor (cat. no. MH19474, Thermo Fisher Scientific, Inc.) using Lipofectamine 3000 Transfection Reagent (Invitrogen; Thermo Fisher Scientific, Inc.) following the manufacturer's protocol. Briefly, Lipofectamine 3000 (2.5 μl/well) was diluted in Opti-MEM (Gibco; Thermo Fisher Scientific, Inc.), and miR inhibitor (10 nM) was mixed in a separate tube with Opti-MEM. The two solutions were combined and incubated at room temperature for 15 min before being added to the cells. Cells were incubated for 6 h at 33˚C, after which the medium was replaced with fresh high-glucose DMEM with 10% FBS, followed by incubation for 24 h before subsequent treatments. For Mdivi-1 pretreatment, cells were pretreated with 10 μM Mdivi-1 (cat. no. S7162, Selleck Chemicals) for 1 h at 33˚C before the addition of D-gal (20 mg/ml, 72 h). Control groups were treated with DMSO (0.1%) as a vehicle control.

Reverse transcription-quantitative (RT-q)PCR. Total RNA from cells and tissues was extracted using TRIzol® (Invitrogen; Thermo Fisher Scientific, Inc.), and cDNA was synthesized with PrimeScript RT Master Mix (cat. no. RR036B; Takara Biotechnology, Ltd.), according to the manufacturers' protocols. The cDNA underwent qPCR with Power UP SYBR Green Master Mix (cat. no. A25742, Thermo Fisher Scientific, Inc.) on an Analytik Jena qTOWER (Analytik Jena GmbH). The amplification conditions for qPCR were as follow: 50˚C for 2 min and 95˚C for 5 min, followed by 40 cycles at 95˚C for 15 sec and 60˚C for 1 min, with a melt curve stage of 95˚C for 15 sec, 60˚C for 1 min and 95˚C for 15 sec. The relative mRNA expression levels of all genes were normalized to β-actin or U6 and were calculated using the 2-ΔΔCq method (17). The primers (Table I) were synthesized by Shanghai GenePharma Co., Ltd.

Intracellular reactive oxygen species (ROS) detection. Intracellular ROS levels were detected by DCFH-DA (Beyotime Institute of Biotechnology) according to the manufacturer's protocols. FACS Calibur system (BD Biosciences) with FlowJo (FlowJo 7.6.1; BD Biosciences) was used to measure fluorescence intensity. The experiment was repeated ≥3 times.

Apoptosis analysis. Annexin V-FITC kit (Beyotime Institute of Biotechnology) was used for apoptosis analysis according to the manufacturer's instructions. The cells were collected by centrifugation (1,000 g, 5 min, 4˚C) and resuspended. FACS Calibur system (BD Biosciences) with FlowJo software (FlowJo 7.6.1; BD Biosciences) was used to measure fluorescence intensity. Cells that were Annexin V-positive and PI-negative were identified as apoptotic. The experiment was repeated ≥3 times.

Western blot analysis. Total protein from cells and tissue was extracted using RIPA lysis buffer (Beyotime Institute of Biotechnology) and the protein concentration was quantified using the BCA Protein Assay kit. The samples (30 μg/lane) were subjected to 10% SDS-PAGE and transferred to polyvinylidene difluoride membranes. Following blocking with 5% bovine serum albumin (Gibco; Thermo Fisher Scientific, Inc.) in TBST (0.1%) for 30 min, they were incubated with the following primary antibodies (1:1,000) in 4˚C overnight: Rabbit anti-superoxide dismutase type 1 (SOD1; cat. no. A22594;

Table I. List of primer sequences.

Gene	Forward primer (5' → 3')	Reverse primer (5' → 3')
mmu-miR-140-5p	CAGTGGTTTTACCCTATGGTAG	GTGCAGGGTCCGAGGT
mmu-miR-141-3p	TAACACTGTCTGGTAAAGATGG	GTGCAGGGTCCGAGGT
mmu-miR-15a-5p	TAGCAGCACATAATGGTTTGUG	GTGCAGGGTCCGAGGT
mmu-miR-34a-5p	TGGCAGTGTCTTAGCTGGTTGT	GTGCAGGGTCCGAGGT
mmu-miR-130a-3p	CAGTGCAATGTTAAAAGGGCAT	GTGCAGGGTCCGAGGT
mmu-miR-148a-3p	TCAGTGCATCACAGAACTTTGT	GTGCAGGGTCCGAGGT
mmu-miR-17-5p	CAAAGTGCTTACAGTGCAGGTAG	GTGCAGGGTCCGAGGT
mmu-miR-574-5p	TGAGTGTGTGTGTGTGTGTGTGA	GTGCAGGGTCCGAGGT
mmu-miR-446a	GCTGTTAATGCTAATCGTGATT	GTGCAGGGTCCGAGGT
mmu-miR-22-3p	AACTGCCTGGTCCAACCTCTAAG	GTGCAGGGTCCGAGGT
mmu-miR-455-3p	GCGACAATGAAGAATTGCCCG	GTGCAGGGTCCGAGGT
mmu-miR-148a-3p	TCAGTGCATCACAGAACTTTGT	GTGCAGGGTCCGAGGT
mmu-miR-27a-3p	ACTGTTGCTGCAGGGTCTTAGC	GTGCAGGGTCCGAGGT
mmu-miR-364-3p	GCGAAATGGTTCTGGTAGTCTGCT	GTGCAGGGTCCGAGGT
mmu-miR-362-5p	AGGCTGGGAAGGAGTGGTTGGA	GTGCAGGGTCCGAGGT
U6	CTCGCTTCGGCAGCACA	AACGCTTCACGAATTTGCGT
TFAM	GCCTGGATCTCTGCAGAACT	GTTGCTTTTTTCCACTCCCTG
β-actin	GGCTGTATTCCCCTCCATCG	CCAGTTGGTAACAATGCCATGT

ABclonal Biotech Co., Ltd.), anti-NLRP3 (A24294, ABclonal Biotech Co., Ltd.), anti-Apoptosis-associated speck-like protein containing a CARD (ASC, cat. no. A22046; ABclonal Biotech Co., Ltd.), anti-caspase1 (cat. no. A23429, ABclonal Biotech Co., Ltd.), anti-pro-caspase1 (cat. no. A21085, ABclonal Biotech Co., Ltd.), anti-dynamin-related protein 1 (DRP1; cat. no. A21968, ABclonal Biotech Co., Ltd.), anti-phosphorylated DRP1 (Ser616; cat. no. 4494, Cell Signaling Technology, Inc.), anti-TFAM (cat. no. A13552, ABclonal Biotech Co., Ltd.) and anti-β-actin (cat. no. AC026, ABclonal Biotech Co., Ltd.). After that, the membranes were incubated with HRP-conjugated secondary antibodies (cat. no. AS014, ABclonal Biotech Co., Ltd. 1:1,000 diluted in TBST) in room temperature for 1 h and were then washed with TBST for three times. The relative protein expression levels were normalized to β-actin. The signals were detected using the ECL Immobilon Western Chemilum HRP Substrate (cat. no. WBKLS0500; Merck Millipore) and an ultra-high sensitivity chemiluminescence imaging system (Bio-Rad Laboratories, Inc.) and quantified using ImageJ 1.48v software (National Institutes of Health).

Cell counting kit (CCK)-8 assay. HEI-OC1 cells were seeded into 96-well plates at a density of 5,000 cells/well and cultured for 24 h. After three washes with PBS, 10 μl CCK-8) reagent (C0005, TargetMol) was added to each well, and the cells were then incubated at 37˚C for another 1 h. The absorbance was measured at an optical density of 450 nm using a microplate reader (Thermo Fisher Scientific, Inc.).

Mitochondrial membrane potential (MMP). MMP was detected using MMP assay kit with JC-1 (cat. no. C2003S, Beyotime Institute of Biotechnology) following the manufacturer's instructions. Cells were viewed under an inverted light microscope (Olympus Corporation; cat. no. X51). Fluorescence intensity was analyzed using ImageJ 1.48v software (National Institutes of Health).

Dual-luciferase reporter assay. The dual-luciferase reporter assay was performed to evaluate the activity of wild-type (WT) and mutant (MUT) TFAM 3'UTR in HEI-OC1 cells under mimic NC or miR-43a mimic treatment. The 3'UTR of mouse TFAM was cloned into the pGL3-Basic luciferase reporter vector (Promega Corporation). To create the mutant construct, the miR-43a binding site in the TFAM 3'UTR was mutated using a site-directed mutagenesis kit (QuickChange Site-Directed Mutagenesis Kit, Agilent). HEI-OC1 cells were cultured in DMEM supplemented with 10% FBS (Gibco; Thermo Fisher Scientific, Inc.) at 33˚C in 5% CO_2. Cells were seeded in 24-well plates at approximately 70-80% confluence. Transfections were performed using Lipofectamine 3,000 (Invitrogen) according to the manufacturer's protocol. The following groups were transfected: pGL3-TFAM-WT + mimic NC, pGL3-TFAM-WT + miR-43a mimic, pGL3-TFAM-MUT + mimic NC, pGL3-TFAM-MUT + miR-43a mimic. Each well was co-transfected with 0.5 μg of the luciferase reporter plasmid and 0.05 μg of Renilla luciferase plasmid (pRL-TK, Promega) as an internal control. After 24-48 h of transfection, cells were lysed using Passive Lysis Buffer (Promega). Firefly and Renilla luciferase activities were measured using the Dual-Luciferase Reporter Assay System (Promega) following the manufacturer's instructions. Luminescence was detected using a microplate reader.

Immunofluorescence staining. The tissue and cells were collected and embedded in paraffin resin before sectioning at a thickness of 5 μm using a microtome. For antigen retrieval, sections were heated to 95˚C for 15 min in citrate buffer (pH 6.0), followed by washing in xylene and rehydration

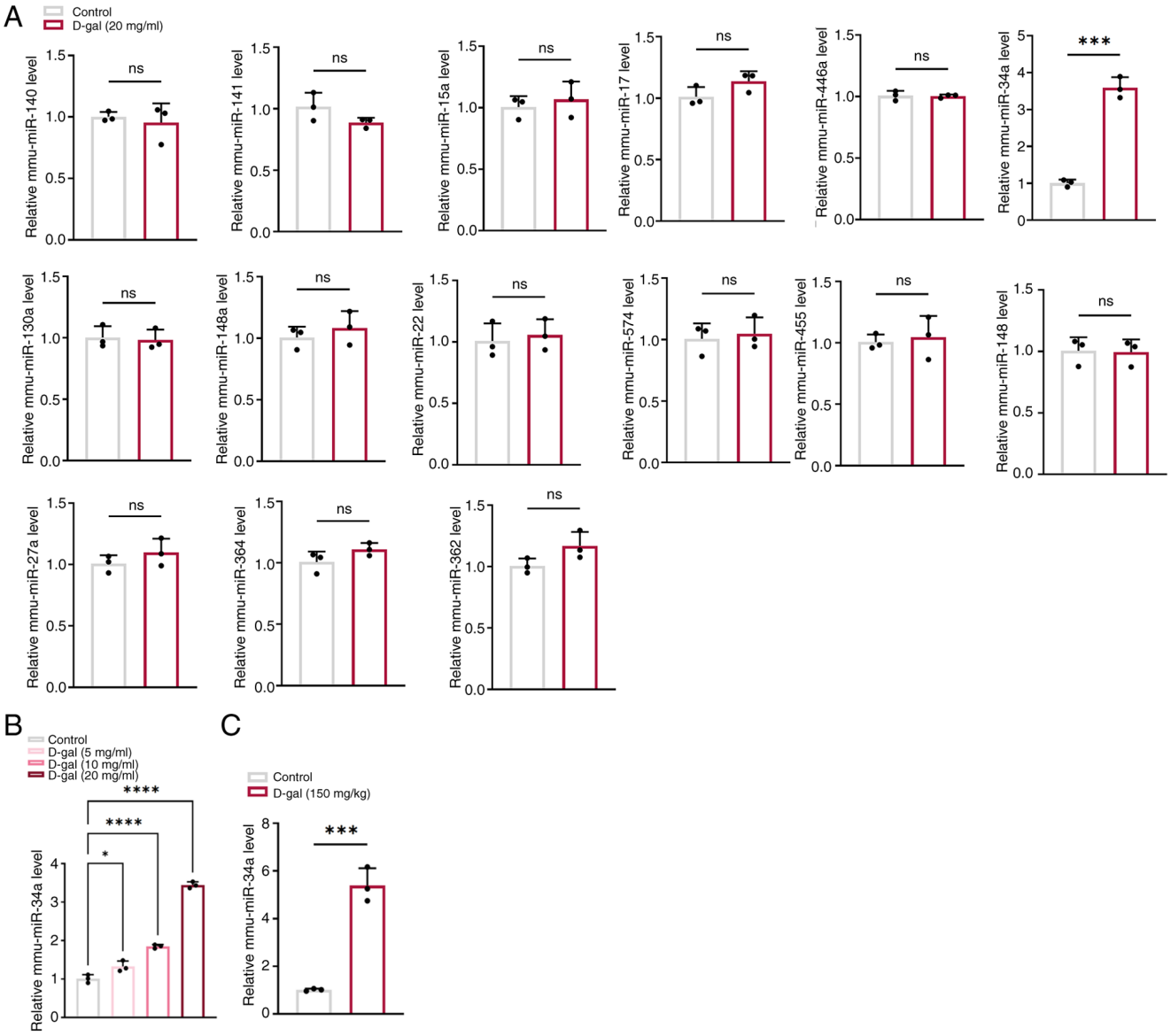

Figure 1. Expression of miRs in D-gal-induced HEI-OC1 cells and cochleae of C57BL/6 mice. (A) Expression of miRs in HEI-OC1 cells exposed to 20 mg/ml D-gal for 72 h. (B) Expression of miR-34a in HEI-OC1 cells exposed D-gal for 72 h. (C) Expression of miR-34a in D-gal-induced aging cochleae of C57BL/6 mice. n=8. miR, microRNA; D-gal, D-galactose; HEI-OC1, House Ear Institute-Organ of Corti 1. ns, not significant. *P<0.05; ***P<0.001; ****P<0.0001.

through a descending alcohol series (100, 95, 85, 70%) into distilled water. After fixation in 4% paraformaldehyde for 30 min at room temperature, samples were blocked with 5% bovine serum albumin (Gibco; Thermo Fisher Scientific, Inc.) at 33˚C for 30 min and incubated overnight at 4˚C with primary antibodies: anti-phosphorylated DRP1 (Ser616; cat. no. 3455, Cell Signaling Technology, Inc.), anti-myosin VIIA (Myo7a, cat. no. 3402, Cell Signaling Technology, Inc.), anti-TFAM (cat. no. 8076, Cell Signaling Technology, Inc.), and anti-gasdermin D (GSDMD, Thermo Fisher Scientific, Inc.). Primary antibodies were diluted at 1:200 in blocking buffer. The tissue and cells were then incubated with a fluorochrome-conjugated secondary antibody (1:500 dilution) for 1 h at room temperature. Samples were visualized under a fluorescence microscope (Olympus Corporation; cat. no. X51) at 40x magnification. Image analysis and fluorescence intensity quantification were performed using ImageJ software (version 1.48v; National Institutes of Health).

Statistical analysis. All data are presented as the mean ± SEM and each experiment was performed in triplicate. Statistical analyses were performed using R (version R-3.4.3). Unpaired Student's t-test was used to compare two groups. One-way analysis of variance followed by Tukey's post hoc test was used to compare >2 groups. P<0.05 was considered to indicate a statistically significant difference.

Results

miR-34a is upregulated in D-gal-induced HEI-OC1 cells and cochleae of C57BL/6 mice. A total of 15 miRNAs including miR-140, miR-141, miR-15a, miR-34a, miR-130a, miR-148a, miR-17, miR-574, miR-446a, miR-22, miR-455, miR-148a, miR-27a, miR-364 and miR-362 were selected from our previous study (18) to identify the key miRNAs involved in D-gal-induced aging. Among these, miR-34a was the only miRNA that was significantly increased in D-gal-induced

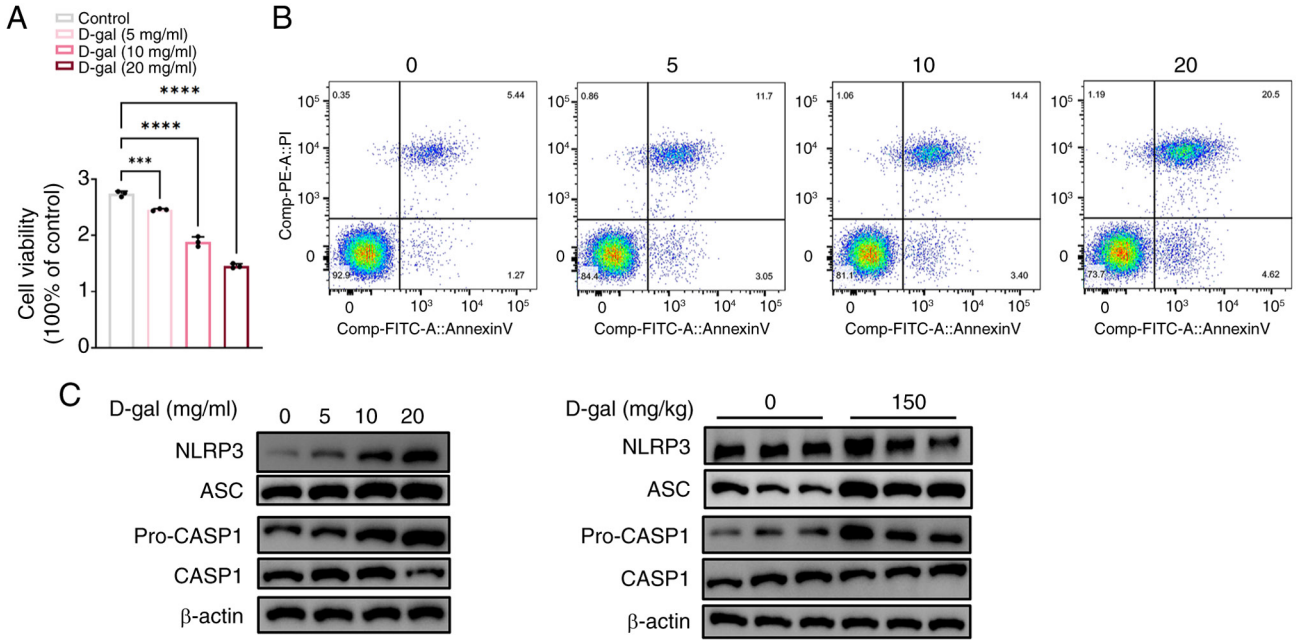

Figure 2. D-gal induces apoptosis and pyroptosis in HEI-OC1 cells. (A) HEI-OC1 cell viability following exposure to D-gal. (B) Flow cytometry of Annexin V/PI double-stained HEI-OC1 cells exposed to D-gal. (C) Western blot analysis of pyroptosis-associated proteins in HEI-OC1 cells exposed to D-gal for 72 h and D-gal-induced aging cochleae of C57BL/6 mice (n=8). D-gal, D-galactose; HEI-OC1, House Ear Institute-organ of Corti 1; ASC, Apoptosis-associated speck-like protein containing a CARD; CASP, Caspase. ***P<0.005; ****P<0.001.

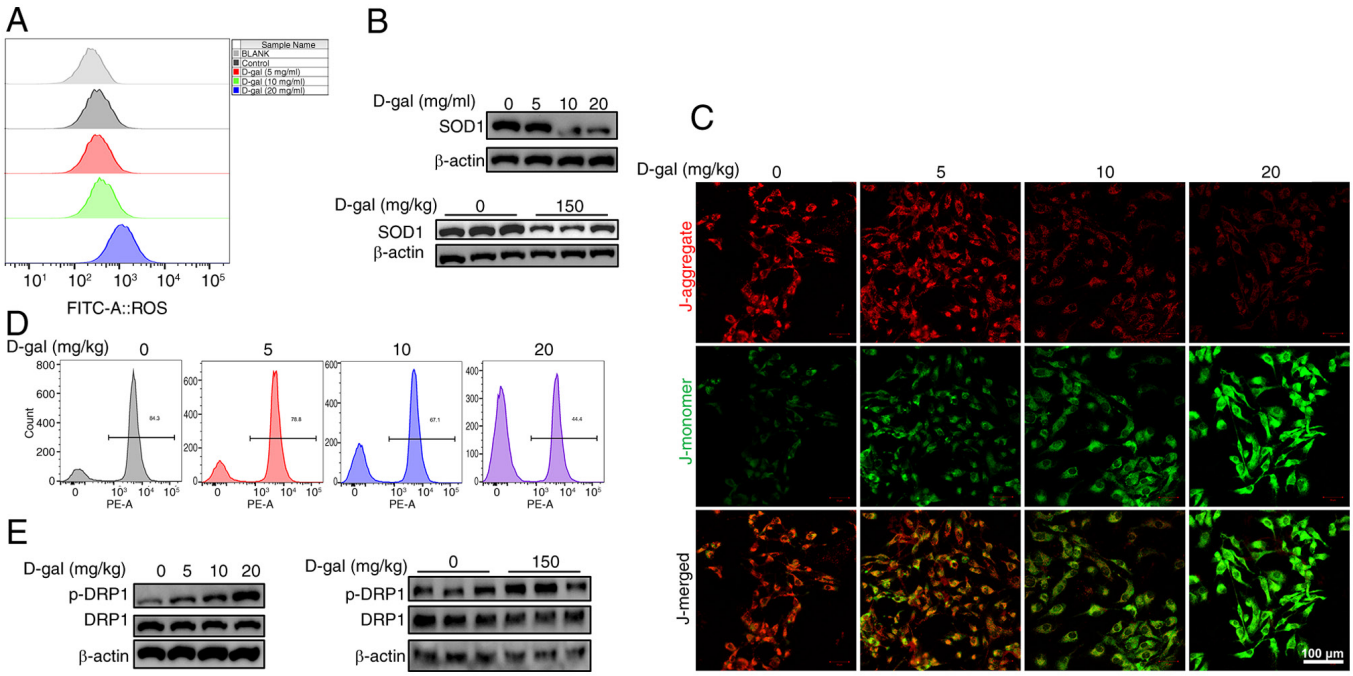

Figure 3. D-gal induces oxidative damage and mitochondrial dysfunction in HEI-OC1 cells. (A) ROS production. (B) Western blot analysis of SOD1 expression. (C) Mitochondrial membrane potential. (D) Flow cytometry result of mitochondrial membrane potential. (E) Western blot analysis of DRP1 phosphorylation *in vitro* and *in vivo* (n=3). Scale bar, 50 μm. D-gal, D-galactose; HEI-OC1, House Ear Institute-Organ of Corti 1; ROS, reactive oxygen species; SOD, superoxide dismutase; DRP, dynamin-related protein 1; p-, phosphorylated.

HEI-OC1 cells compared with controls (Fig. 1A) and the expression of miR-34a was positively associated with concentration of D-gal (Fig. 1B), suggesting that miR-34a may play a key role in D-gal-induced aging in HEI-OC1 cells. This was confirmed in cochleae of D-gal-induced aging C57BL/6 mice as miR-34a significantly increased in D-gal treated mice compared with the control (Fig. 1C).

D-gal induces apoptosis and pyroptosis in HEI-OC1 cells. The effect of D-gal was assessed using the Cell Counting Kit-8 assay (Fig. 2A). HEI-OC1 cell viability decreased in a dose-dependent manner, consistent with the flow cytometry results (Fig. 2B). Annexin V-positive staining increased with increasing D-gal concentration, indicating increased apoptotic cells (Fig. 2B). Compared with the control groups, the expression of four key

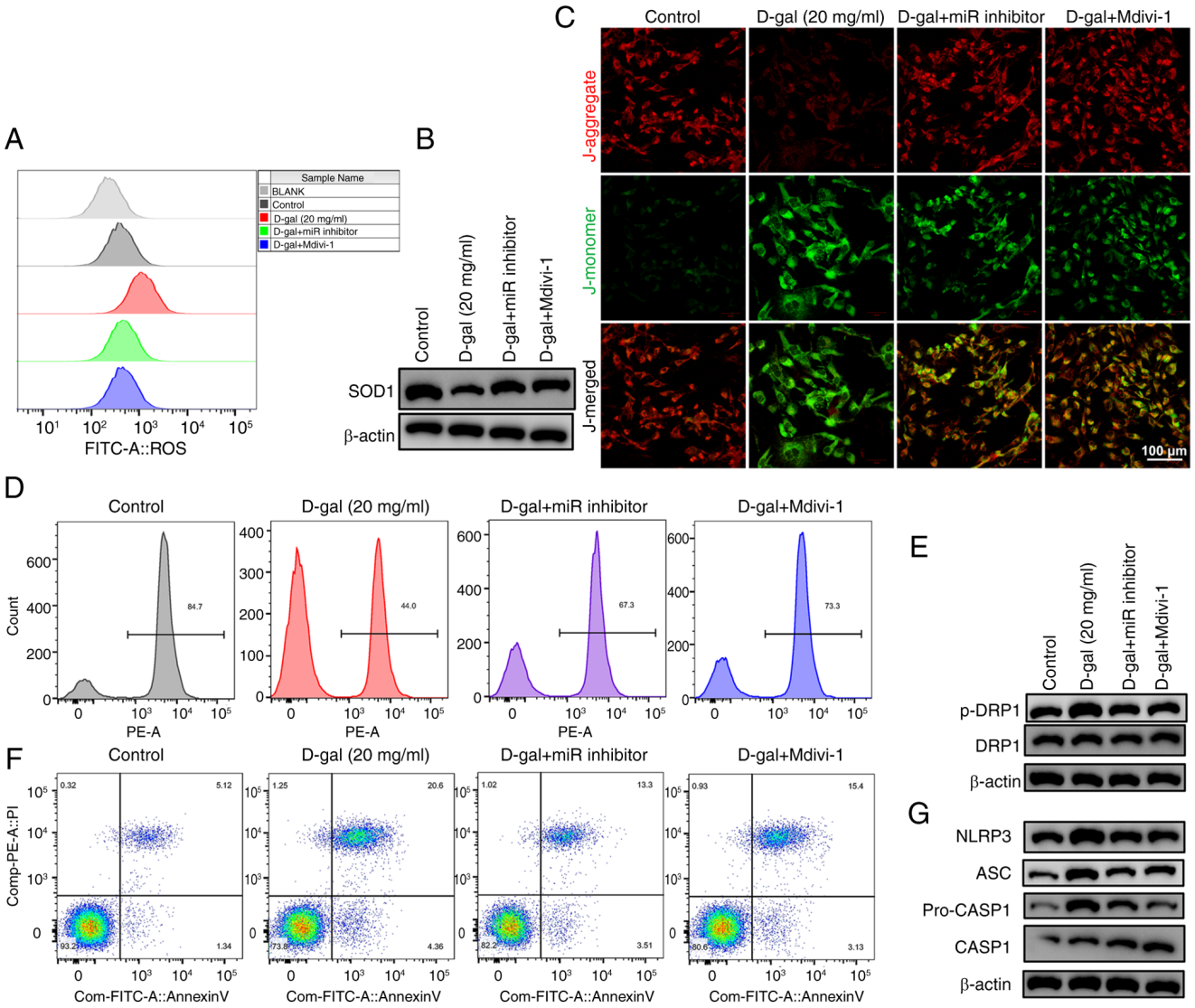

Figure 4. Effect of miR inhibitor and Mdivi-1 on mitochondrial dysfunction, apoptosis and pyroptosis in D-gal-induced HEI-OC1 cells. (A) ROS production. (B) Western blot analysis of SOD1 expression. (C) Immunostaining of (D) mitochondrial membrane potential. Scale bar, 50 μm. (E) Western blot analysis of DRP1 phosphorylation. (F) Flow cytometry results of Annexin V/PI double-stained HEI-OC1 cells. (G) Western blot analysis of pyroptosis-related proteins in HEI-OC1 cells. miR, microRNA; D-gal, D-galactose; HEI-OC1, House Ear Institute-Organ of Corti 1; ROS, reactive oxygen species; SOD, superoxide dismutase; DRP, dynamin-related protein 1; p-, phosphorylated; ASC, apoptosis-associated speck-like protein containing a CARD; CASP, caspase.

pyroptosis-related proteins, pro-caspase1, caspase1, ASC and NLRP3, significantly increased in HEI-OC1 cells after exposure D-gal for 72 h (Fig. 2C) in a dose-dependent manner. These results indicate that D-gal induces apoptosis and pyroptosis in HEI-OC1 cells. The upregulation of pyroptosis-associated proteins was confirmed in the aging cochleae of D-gal-induced C57BL/6 mice (Fig. 2C).

D-gal induces oxidative damage and mitochondrial dysfunction in HEI-OC1 cells. Similar to what is hypothesized to occur in ARHL, the mechanism underlying D-gal-induced and natural aging is oxidative stress resulting from excessive ROS production and imbalance between excessive ROS and the antioxidant system (19,20). ROS levels in HEI-OC1 cells following 5, 10, and 20 mg/ml D-gal exposure for 72 h was assessed by DCFH-DA staining and the expression of the antioxidant enzyme SOD1, an enzyme that protects the cells from excessive ROS (21), was detected using western blot analysis. Fluorescence intensity of ROS notably increased with increasing D-gal concentration (Fig. 3A), accompanied by a decrease in SOD1 levels (Fig. 3B), suggesting enhanced ROS production and insufficient antioxidant system after D-gal exposure. As mitochondria are the primary source of ROS and are susceptible to oxidative damage (22), the present study investigated whether mitochondrial function was compromised following exposure to D-gal. Mitochondrial integrity and bioenergetic function were assessed by MMP analysis using immunofluorescence staining and flow cytometry. Immunofluorescence staining revealed a notable increase in the number of green-stained cells (indicating damaged mitochondria), while the number of red-stained cells (representing healthy mitochondria) notably decreased (Fig. 3C). This was consistent with flow cytometry results, where nearly half of the mitochondria in HEI-OC1 cells exposed to 20 mg/ml D-gal were damaged compared with the control (Fig. 3D), indicating disrupted mitochondrial dynamics in D-gal-induced HEI-OC1

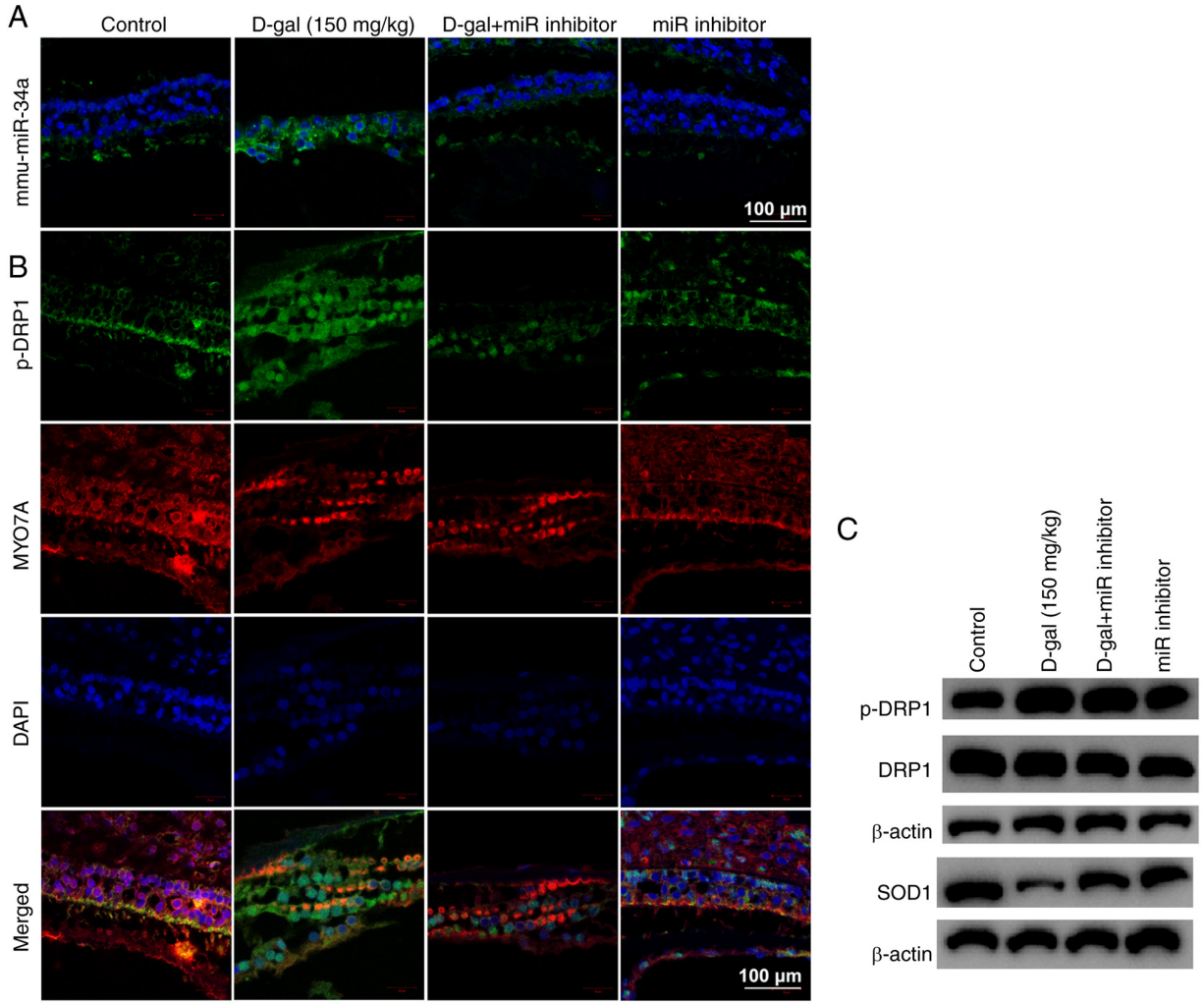

Figure 5. miR inhibitor inhibits oxidative damage and reverses mitochondrial dysfunction in D-gal-induced cochleae of C57BL/6 mice. Representative (A) miR-34a (green) and (B) Myo7A (hair cell-specific, red), p-DRP1 (green) and DAPI (nuclear-specific dye, blue) staining. n=8. (C) Western blot analysis of SOD1 expression and DRP1 phosphorylation. n=3. Scale bar, 20 μm. miR, microRNA; D-gal, D-galactose; Myo7A, ; SOD, superoxide dismutase; p-DRP, phosphorylated dynamin-related protein 1.

cells. DRP1 is a key component of mitochondrial fission, representing the normal function of mitochondria, and a downstream protein of miR-34a (23,24). Western blot analysis (Fig. 3E) demonstrated a notable increase in DRP1 phosphorylation, indicating activation in D-gal-induced HEI-OC1 cells and the cochleae of C57BL/6 mice, implying excessive mitochondrial fission and dysfunction.

miR-34a inhibitor improves apoptosis and pyroptosis induced by D-gal in HEI-OC1 cells via inhibiting mitochondrial dysfunction. To investigate the role of miR-34a and mitochondrial dysfunction in D-gal-induced aging process, HEI-OC1 cells were either transfected with a miR inhibitor (to inhibit miR-34a) or pretreated with Mdivi-1 (to inhibit DRP1). miR inhibitor and Mdivi-1 significantly reversed oxidative damage, mitochondrial dysfunction, apoptosis and pyroptosis in D-gal-induced HEI-OC1 cells (Fig. 4), indicating miR-34a is a key element in promoting apoptosis and pyroptosis through mitochondrial dysfunction. In mouse cochleae, miR inhibitor decreased miR-34a expression (Fig. 5A) and DRP1 phosphorylation and increased SOD1 (Fig. 5B and C). Immunostaining (Fig. 5B) confirmed that there was an overlap between cells expressing phosphorylated DRP1 and hair cell-specific marker Myo7A. Taken together, these data validated the role of miR-34a in D-gal-induced aging process *in vivo*.

miR-34a regulates aging process via inhibiting TFAM in D-gal-induced HEI-OC1 cells and cochleae of C57BL/6 mice. Based on several studies (25,26), it was hypothesized that TFAM might be the target gene of miR-34a based on putative target sequences of TFAM localized in the 3' untranslated region (Fig. 6A). A dual luciferase reporter assay provided direct evidence for the interaction between miR-34a and TFAM (Fig. 6B). Western blot analysis revealed that miR-34a inhibited protein expression of TFAM (Fig. 6D) while transcription of TFAM was promoted (Fig. 6C). Expression of TFAM exhibited a notable decrease after exposure to D-gal (Fig. 6E and F). Furthermore, the decrease was reversed by miR 34a inhibitor, indicating the downstream inhibitory effect of miR-34a on TFAM.

TFAM was silenced to verify its involvement in mitochondrial dysfunction, apoptosis and pyroptosis induced by D-gal in HEI-OC1 cells. The protective effect of miR-inhibitor was notably reduced by the interference of TFAM in D-gal-induced

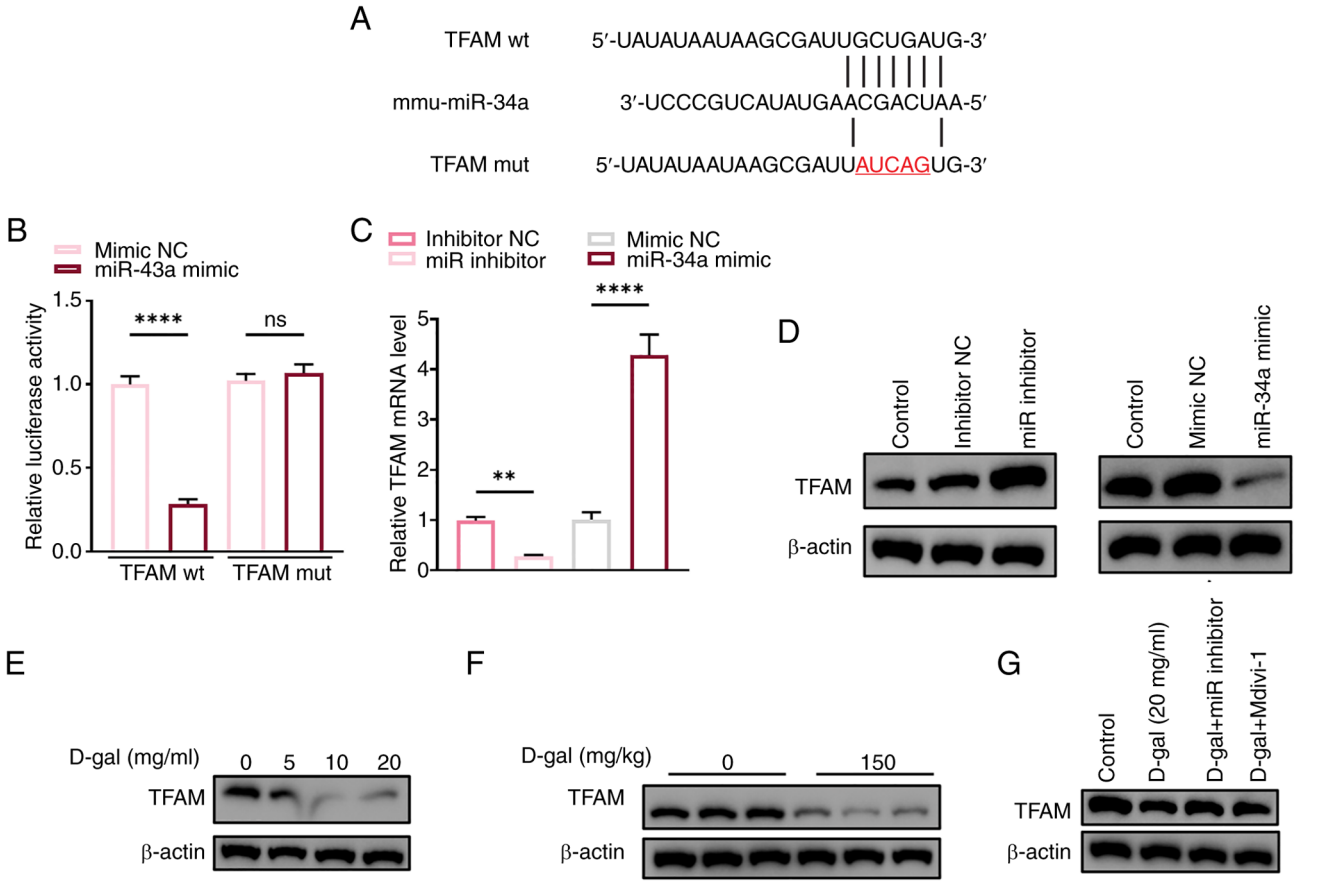

Figure 6. Interaction of miR-34a with TFAM and TFAM expression in HEI-OC1 cells and cochleae of C57BL/6 mice. (A) Putative binding site of miR-34a. (B) Dual-luciferase activity of miR-34a and TFAM. TFAM (C) mRNA and (D) protein expression in HEI-OC1 cells. TFAM protein expression in (E) HEI-OC1 cells and (F) D-gal-induced aging cochleae of C57BL/6 mice (n=3). (G) Western blot analysis of TFAM expression in HEI-OC1 cells. miR, microRNA; TFAM, mitochondrial transcription factor A; HEI-OC1, House Ear Institute-organ of Corti 1; NC, negative control; wt, wild-type; mut, mutant. ns, not significant; **P<0.01; ****P<0.001.

HEI-OC1 cells (Fig. 7): Oxidative stress and mitochondrial damage, proportion of annexin V-positive D-gal-induced HEI-OC1 cells and expression levels of pyroptosis-associated NLRP3, ASC, caspase1 and p-caspase1 notably increased, indicating TFAM is a key component of the aging process induced by D-gal. Furthermore, there was colocalization of TFAM with GSDMD *in vitro* and *in vivo* (Fig. 7G and H), suggesting TFAM may serve a key role in D-gal-induced pyroptosis as GSDMD is crucial for pyroptosis.

Discussion

D-gal is used to accelerate aging in mammalian cochlea and investigate the underlying mechanism of ARHL (11). As ARHL is currently irreversible, progressive and untreatable (4), the present study aimed to elucidate the key components underlying its molecular pathogenesis to identify potential treatment targets. miRNAs have recently gained increasing interest (27-29) in hearing loss due to their potential involvement in auditory development, cochlear homeostasis maintenance and pathological processes of hearing loss. The present study investigated the role of miR-34a in ARHL using D-gal-induced aging in HEI-OC1 cells and C57BL/6 mice and suggested that miR-34a may serve as a potential therapeutic target for ARHL.

Cochlear hair cell loss is the leading cause of sensory deficit in ARHL (5). By applying D-gal to HEI-OC1 cells and C57BL/6 mice, cell loss, apoptosis and mitochondrial dysfunction were induced, similar to other studies (7,11). Oxidative stress/mitochondrial dysfunction-induced apoptosis are hypothesized to be the main contributors to hair cell death. Inflammation may also contribute to ARHL (2,4). With aging, patients with ARHL present a gradual increase in systemic inflammation with a decrease in hearing thresholds (30). This suggests inflammation serves a vital role in ARHL progression and pyroptosis, a programmed cell death triggered by inflammatory cystathionases, may be involved in cochlear hair cell loss during aging (31). Here, pyroptosis-associated NLRP3, ASC, caspase1 and pro-caspase1 were upregulated in both D-gal-induced *in vitro* and *in vivo* aging models, suggesting that pyroptosis contributes to aging cochlear hair cell loss and apoptosis. This is in line with recent studies (31,32), which found pyroptosis to be a key element in ARHL.

miR-34a has recently been found to serve as a key regulator of different types of hearing loss (28,31,33). Apart from modulating autophagy and contributing to cochlear hair cell apoptosis in ARHL (34,35), miR-34a participates in cisplatin-induced ototoxicity via mediating mitophagy (36). In the present study, miR-34a was identified in a miRNA screen

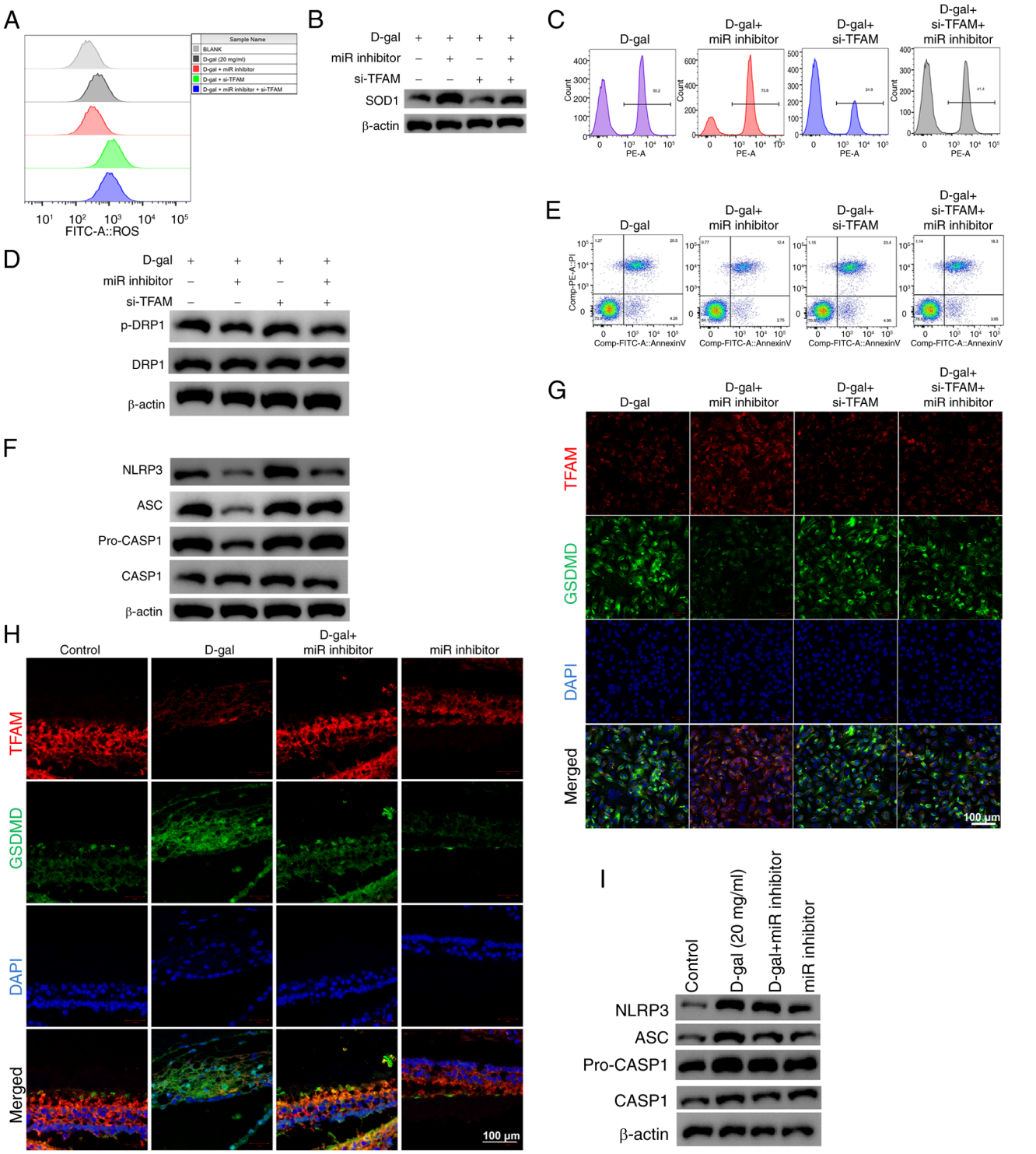

Figure 7. Effect of TFAM on D-gal-induced mitochondrial dysfunction, apoptosis and pyroptosis in HEI-OC1 cells. (A) ROS production. (B) Western blot analysis of SOD1 expression. (C) Mitochondrial membrane potential. (D) Western blot analysis of DRP1 phosphorylation. (E) Effect of TFAM and miR-34a on early apoptosis. (F) Western blot analysis of pyroptosis-associated proteins. Representative TFAM (red), GSDMD (green), and DAPI (blue)-staining of (G) HEI-OC1 cells (scale bar, 50 μm) and (H) D-gal-induced cochleae. n=8. Scale bar, 20 μm. (I) Western blot analysis of pyroptosis-associated proteins in D-gal-induced cochleae (n=3). TFAM, mitochondrial transcription factor A; D-gal, D-galactose; HEI-OC1, House Ear Institute-Organ of Corti 1; ROS, reactive oxygen species; SOD, superoxide dismutase; DRP, dynamin-related protein 1; miR, microRNA; GSDMD, gasdermin D; si, small interfering; p-, phosphorylated; CASP, caspase; ASC, Apoptosis-associated speck-like protein containing a CARD.

based on five ARHL databases in our previous study (18). This was consistent with previous studies that have revealed miR-34a as a vital regulator of age-dependent tissue changes and a cell senescence inducer (37-39). miR-34a increases with age in several organs such as heart and blood vessels and serves a key role in age-associated functional impairment. By applying the miR-inhibitor, mitochondrial dysfunction, apoptosis and pyroptosis were reversed *in vitro* and *in vivo*, suggesting that miR-34a served as a key modulator of the aging process.

Apoptosis and pyroptosis were notably decreased when cells were pretreated with Mdivi-1, a DRP1 inhibitor. Since DRP1 represents the normal function of mitochondria, this indicates that miR-34a modulates apoptosis and pyroptosis via mitochondrial dysfunction. miR-34a and mitochondrial apoptosis are associated; miR-34a was first described as a p53-induced tumor suppressor miRNA that controls apoptosis and senescence of tumor cells (40) and directly targets antioxidative genes (41). miR-34a inhibits sirtuin 3 expression, aggravates pyroptosis (42,43) and is considered to be associated with inflammation (44). However, there are cross-talk pathways between mitochondrial apoptosis and pyroptosis (45,46), but these interactions require further elucidation.

TFAM is a key mitochondrial DNA (mtDNA) packaging protein whose disruption may lead to mtDNA depletion and mitochondrial dysfunction (47), which can lead to aging (48,49). TFAM deficiency has been recognized as an accelerator of senescence (50,51), but not yet in ARHL. The present study demonstrated that miR-34a inhibited TFAM to regulate apoptosis and pyroptosis in D-gal-induced aging HEI-OC1 cells and cochleae. The present results demonstrated a negative association between miR-34a and its target TFAM in D-gal-induced aging HEI-OC1 cells and cochleae, suggesting miR-34a exerts pro-death effects by targeting TFAM, thus inhibiting its antioxidative functions. TFAM expression was found to be decreased and to serve a protective role in noise-exposed (52) and cisplatin-induced (53) cochleae but increased and damages cells in D-gal-induced cochlea (54) and auditory cortex (6). This may be because the concentration of D-gal in the aforementioned experiments was relatively high (500 mg/kg). However, miR-34a may lose its inhibitory effect on TFAM and TFAM may serve a pro-death role with high concentrations of D-gal. The present study observed colocalization of TFAM and the pyroptotic protein GSDMD *in vitro* and *in vivo*, suggesting that TFAM may serve a key role in pyroptosis, but more detailed research including RNA pull-down assay to verify the binding, is needed.

In conclusion, miR-34a is a key regulator of apoptosis and pyroptosis in D-gal-induced aging HEI-OC1 cells and cochleae of C57BL/6 mice via inhibition of TFAM, thus promoting mitochondrial dysfunction. The present results improve understanding of miR-34a-mediated cochlear hair cell loss in ARHL development and suggest miR-34a as a promising therapeutic target for ARHL treatment.

Acknowledgements

Not applicable.

Funding

The present study was supported by Ningxia Natural Science Foundation (grant no. 2021AAC03297) and Ningxia Hui Autonomous Region Key Research and Development Program Project (grant no. 2022BEG03163).

Availability of data and materials

The data generated in the present study may be requested from the corresponding author.

Authors' contributions

YW performed experiments. YW and GW wrote the manuscript. MY and BD performed experiments. GW constructed figures. WL designed the methodology. BD and GW analyzed data. XY and XL conceived the study. XL and GW edited the manuscript. YW and XL confirm the authenticity of all the raw data. All authors have read and approved the final manuscript.

Ethics approval and consent to participate

The present study was approved by animal care and the Ethics Committee for Animal Research (2020-NZR-037, People's Hospital of Ningxia Hui Autonomous Region, Yinch.

Patient consent for publication

Not applicable.

Competing interests

The authors declare that they have no competing interests.

References

1. World Health Organization. World Report on Hearing. World Health Organization, Geneva, 2021.
2. Gates GA and Mills JH: Presbycusis. Lancet 366: 1111-1120, 2005.
3. Rutherford BR, Brewster K, Golub JS, Kim AH and Roose SP: Sensation and psychiatry: Linking age-related hearing loss to late-life depression and cognitive decline. Am J Psychiatry 175: 215-224, 2018.
4. Bowl MR and Dawson SJ: Age-related hearing loss. Cold Spring Harb Perspect Med 9: a033217, 2019.
5. Wu PZ, O'Malley JT, de Gruttola V and Liberman MC: Age-related hearing loss is dominated by damage to inner ear sensory cells, not the cellular battery that powers them. J Neurosci 40: 6357-6366, 2020.
6. Zhong Y, Hu Y, Peng W, Sun Y, Yang Y, Zhao X, Huang X, Zhang H and Kong W: Age-related decline of the cytochrome c oxidase subunit expression in the auditory cortex of the mimetic aging rat model associated with the common deletion. Hear Res 294: 40-48, 2012.
7. Du Z, Yang Y, Hu Y, Sun Y, Zhang S, Peng W, Zhong Y, Huang X and Kong W: A long-term high-fat diet increases oxidative stress, mitochondrial damage and apoptosis in the inner ear of D-galactose-induced aging rats. Hear Res 287: 15-24, 2012.
8. Yu J, Wang Y, Liu P, Li Q, Sun Y and Kong W: Mitochondrial DNA common deletion increases susceptibility to noise-induced hearing loss in a mimetic aging rat model. Biochem Biophys Res Commun 453: 515-520, 2014.
9. Parameshwaran K, Irwin MH, Steliou K and Pinkert CA: D-galactose effectiveness in modeling aging and therapeutic antioxidant treatment in mice. Rejuvenation Res 13: 729-735, 2010.
10. Chen B, Zhong Y, Peng W, Sun Y and Kong WJ: Age-related changes in the central auditory system: Comparison of D-galactose-induced aging rats and naturally aging rats. Brain Res 1344: 43-53, 2010.
11. He ZH, Li M, Fang QJ, Liao FL, Zou SY, Wu X, Sun HY, Zhao XY, Hu YJ, Xu XX, *et al*: FOXG1 promotes aging inner ear hair cell survival through activation of the autophagy pathway. Autophagy 17: 4341-4362, 2021.
12. Bartel DP: MicroRNAs: Genomics, biogenesis, mechanism, and function. Cell 116: 281-297, 2004.
13. Wienholds E, Kloosterman WP, Miska E, Alvarez-Saavedra E, Berezikov E, de Bruijn E, Horvitz HR, Kauppinen S and Plasterk RH: MicroRNA expression in zebrafish embryonic development. Science 309: 310-311, 2005.

14. Rudnicki A and Avraham KB: microRNAs: The art of silencing in the ear. EMBO Mol Med 4: 849-859, 2012.
15. Rudnicki A, Isakov O, Ushakov K, Shivatzki S, Weiss I, Friedman LM, Shomron N and Avraham KB: Next-generation sequencing of small RNAs from inner ear sensory epithelium identifies microRNAs and defines regulatory pathways. BMC Genomics 15: 484, 2014.
16. National Research Council: Guide for the Care and Use of Laboratory Animals: 8th edition. The National Academies Press, Washington, DC, pp246, 2011.
17. Livak KJ and Schmittgen TD: Analysis of relative gene expression data using real-time quantitative PCR and the 2(-Delta Delta C(T)) method. Methods 25: 402-408, 2001.
18. Yang X, Wang G, Liu W, Zhang J, Deng B, Li X and Wang L: Key genes and potential drugs in age-related hearing loss: Transcriptome analysis of cochlear hair cells in old mice. Cell Mol Biol (Noisy-le-grand) 69: 67-74, 2023.
19. Fujimoto C and Yamasoba T: Oxidative stresses and mitochondrial dysfunction in age-related hearing loss. Oxid Med Cell Longev 2014: 582849, 2014.
20. Qiu Y, Liu Y and Tao J: Progress of clinical evaluation for vascular aging in humans. J Transl Int Med 9: 17-23, 2021.
21. Fridovich I: Superoxide anion radical (O2-.), superoxide dismutases, and related matters. J Biol Chem 272: 18515-18517, 1997.
22. Kowaltowski AJ, de Souza-Pinto NC, Castilho RF and Vercesi AE: Mitochondria and reactive oxygen species. Free Radic Biol Med 47: 333-343, 2009.
23. Kornfeld OS, Qvit N, Haileselassie B, Shamloo M, Bernardi P and Mochly-Rosen D: Interaction of mitochondrial fission factor with dynamin related protein 1 governs physiological mitochondrial function in vivo. Sci Rep 8: 14034, 2018.
24. Chen KH, Dasgupta A, Lin J, Potus F, Bonnet S, Iremonger J, Fu J, Mewburn J, Wu D, Dunham-Snary K, *et al*: Epigenetic dysregulation of the dynamin-related protein 1 binding partners MiD49 and MiD51 increases mitotic mitochondrial fission and promotes pulmonary arterial hypertension: Mechanistic and therapeutic implications. Circulation 138: 287-304, 2018.
25. Thounaojam MC, Jadeja RN, Warren M, Powell FL, Raju R, Gutsaeva D, Khurana S, Martin PM and Bartoli M: MicroRNA-34a (miR-34a) mediates retinal endothelial cell premature senescence through mitochondrial dysfunction and loss of antioxidant activities. Antioxidants (Basel) 8: 328, 2019.
26. Fan X, Zhou S, Zheng M, Deng X, Yi Y and Huang T: MiR-199a-3p enhances breast cancer cell sensitivity to cisplatin by downregulating TFAM (TFAM). Biomed Pharmacother 88: 507-514, 2017.
27. Ding L and Wang J: MiR-106a facilitates the sensorineural hearing loss induced by oxidative stress by targeting connexin-43. Bioengineered 13: 14080-14093, 2022.
28. Nunez DA and Guo RC: Acquired sensorineural hearing loss, oxidative stress, and microRNAs. Neural Regen Res 20: 2513-2519, 2025.
29. Zhang J, Sun W, Kuang S, Gan Q, Li H, Ma H, Yang G, Guo J, Tang Y and Yuan W: miR-130b-3p involved in the pathogenesis of age-related hearing loss via targeting PPARγ and autophagy. Hear Res 449: 109029, 2024.
30. Verschuur CA, Dowell A, Syddall HE, Ntani G, Simmonds SJ, Baylis D, Gale CR, Walsh B, Cooper C, Lord JM and Sayer AA: Markers of inflammatory status are associated with hearing threshold in older people: Findings from the hertfordshire ageing study. Age Ageing 41: 92-97, 2012.
31. Yang X, Wu Y, Zhang M, Zhang L, Zhao T, Qian W, Zhu M, Wang X, Zhang Q, Sun J and Dong L: Piceatannol protects against age-related hearing loss by inhibiting cellular pyroptosis and inflammation through regulated Caspase11-GSDMD pathway. Biomed Pharmacother 163: 114704, 2023.
32. Zhang A, Pan Y, Wang H, Ding R, Zou T, Guo D, Shen Y, Ji P, Huang W, Wen Q, *et al*: Excessive processing and acetylation of OPA1 aggravate age-related hearing loss via the dysregulation of mitochondrial dynamics. Aging Cell 23: e14091, 2024.
33. Safabakhsh S, Wijesinghe P, Nunez M and Nunez DA: The role of hypoxia-associated miRNAs in acquired sensorineural hearing loss. Front Cell Neurosci 16: 916696, 2022.
34. Xiong H, Pang J, Min X, Ye Y, Lai L and Zheng Y: miR-34a/ATG9A/TFEB signaling modulates autophagy in cochlear hair cells and correlates with age-related hearing loss. Neuroscience 491: 98-109, 2022.
35. Pang J, Xiong H, Lin P, Lai L, Yang H, Liu Y, Huang Q, Chen S, Ye Y, Sun Y and Zheng Y: Activation of miR-34a impairs autophagic flux and promotes cochlear cell death via repressing ATG9A: Implications for age-related hearing loss. Cell Death Dis 8: e3079, 2017.
36. Wang H, Lin H, Kang W, Huang L, Gong S, Zhang T, Huang X, He F, Ye Y, Tang Y, *et al*: miR-34a/DRP-1-mediated mitophagy participated in cisplatin-induced ototoxicity via increasing oxidative stress. BMC Pharmacol Toxicol 24: 16, 2023.
37. Boon RA, Iekushi K, Lechner S, Seeger T, Fischer A, Heydt S, Kaluza D, Tréguer K, Carmona G, Bonauer A, *et al*: MicroRNA-34a regulates cardiac ageing and function. Nature 495: 107-110, 2013.
38. Ito T, Yagi S and Yamakuchi M: MicroRNA-34a regulation of endothelial senescence. Biochem Biophys Res Commun 398: 735-740, 2010.
39. Yang J, Chen D, He Y, Meléndez A, Feng Z, Hong Q, Bai X, Li Q, Cai G, Wang J and Chen X: MiR-34 modulates Caenorhabditis elegans lifespan via repressing the autophagy gene atg9. Age (Dordr) 35: 11-22, 2013.
40. Hermeking H: The miR-34 family in cancer and apoptosis. Cell Death Differ 17: 193-199, 2010.
41. Bai XY, Ma Y, Ding R, Fu B, Shi S and Chen XM: miR-335 and miR-34a Promote renal senescence by suppressing mitochondrial antioxidative enzymes. J Am Soc Nephrol 22: 1252-1261, 2011.
42. Zhong Z, Gao Y, Zhou J, Wang F, Zhang P, Hu S, Wu H, Lou H, Chi J, Lin H and Guo H: Inhibiting mir-34a-5p regulates doxorubicin-induced autophagy disorder and alleviates myocardial pyroptosis by targeting Sirt3-AMPK pathway. Biomed Pharmacother 168: 1156v, 2023.
43. Chen S, Ding R, Hu Z, Yin X, Xiao F, Zhang W, Yan S and Lv C: MicroRNA-34a inhibition alleviates lung injury in cecal ligation and puncture induced septic mice. Front Immunol 11: 1829, 2020.
44. Li C, Qu L, Farragher C, Vella A and Zhou B: MicroRNA regulated macrophage activation in obesity. J Transl Int Med 7: 46-52, 2019.
45. Bao H and Peng A: The green tea polyphenol(-)-epigallocatechin-3-gallate and its beneficial roles in chronic kidney disease. J Transl Int Med 4: 99-103, 2016.
46. Li Q, Shi N, Cai C, Zhang M, He J, Tan Y and Fu W: The role of mitochondria in pyroptosis. Front Cell Dev Biol 8: 630771, 2021.
47. Campbell CT, Kolesar JE and Kaufman BA: Mitochondrial transcription factor A regulates mitochondrial transcription initiation, DNA packaging, and genome copy number. Biochim Biophys Acta 1819: 921-929, 2012.
48. Zhu M, Ding Q, Lin Z, Chen X, Chen S and Zhu Y: New insights of epigenetics in vascular and cellular senescence. J Transl Int Med 9: 239-248, 2021.
49. Wang P, Zhang N, Wu B, Wu S, Zhang Y and Sun Y: The role of mitochondria in vascular calcification. J Transl Int Med 8: 80-90, 2020.
50. Desdín-Micó G, Soto-Heredero G, Aranda JF, Oller J, Carrasco E, Gabandé-Rodríguez E, Blanco EM, Alfranca A, Cussó L, Desco M, *et al*: T cells with dysfunctional mitochondria induce multimorbidity and premature senescence. Science 368: 1371-1376, 2020.
51. Zhao M, Liu S, Wang C, Wang Y, Wan M, Liu F, Gong M, Yuan Y, Chen Y, Cheng J, *et al*: Mesenchymal stem cell-derived extracellular vesicles attenuate mitochondrial damage and inflammation by stabilizing mitochondrial DNA. ACS Nano 15: 1519-1538, 2021.
52. Chen JW, Ma PW, Yuan H, Wang WL, Lu PH, Ding XR, Lun YQ, Yang Q and Lu LJ: mito-TEMPO attenuates oxidative stress and mitochondrial dysfunction in noise-induced hearing loss via maintaining TFAM-mtDNA interaction and mitochondrial biogenesis. Front Cell Neurosci 16: 803718, 2022.
53. Nong H, Song X, Li Y, Xu Y, Wang F, Wang Y, Zhang J, Chen C and Li J: AdipoRon reduces cisplatin-induced ototoxicity in hair cells:possible relation to the regulation of mitochondrial biogenesis. Neurosci Lett 819: 137577, 2024.
54. Zhong Y, Hu YJ, Chen B, Peng W, Sun Y, Yang Y, Zhao XY, Fan GR, Huang X and Kong WJ: Mitochondrial transcription factor A overexpression and base excision repair deficiency in the inner ear of rats with D-galactose-induced aging. FEBS J 278: 2500-2510, 2011.

Copyright © 2025 Wang et al. This work is licensed under a Creative Commons Attribution-NonCommercial-NoDerivatives 4.0 International (CC BY-NC-ND 4.0) License.